(Received 29 September 2025, Accepted 13 November 2025, Scheduled 20 January 2026)

Design and Fabrication of a New Triple-Band Bandpass Filter with Adjustable Bandwidth Passbands Depending on Coupling Transmission Poles with Center Frequencies of SIW Cavity Modes

Obaida Oulad Haddar[1,2], Mohammed Boulesbaa[1,2,*], and Tarek Djerafi[3]

[1] *Department of Electronics and Telecommunications*
University Kasdi Merbah Ouargla, Ouargla 30000, Algeria
[2] *Laboratory of Radiation and Plasmas and Surface Physics (LRPPS)*
University Kasdi Merbah Ouargla, Ouargla, Route de Ghardaia, BP. 511 30000, Algeria
[3] *Centre-Énergie Matériaux Télécommunication*
Institut National de la Recherche Scientifique, Montréal, Québec, Canada

ABSTRACT: In this research, a simple design with a compact size of a triple-band bandpass filter (BPF) based on SIW is proposed. The proposed design consists of a main SIW cavity combined with two others-secondary SIW cavities. The three passbands of the proposed BPF are formed based on the center frequencies (CFs) of the four modes given by the main SIW cavity and two transmission poles (TP_1 and TP_2) achieved with the secondary SIW cavity. The SIW modes achieved with the main SIW cavity are TE_{101}, TE_{201}, and TE_{301} addition to the suppressed mode, and those modes are realized by the perturbation of seven metallic vias. The coupling of the TP_1 with the suppressed mode realizes the first passband of the filter proposed with a bandwidth of 0.53 GHz. Vertical CPW slots are etched at the main SIW cavity for coupling TE_{101} and TE_{201} to form the second passband with a bandwidth of 1.3 GHz. Horizontal CPW slots are etched in the two rectangular secondary SIW cavities to join the TP_2 with TE_{301} mode for realizing the third passband with a bandwidth of 1.2 GHz. Finally, an adjustable bandwidth filter with CFs of 6.9/10.1/13.3 GHz, respectively, has been achieved. Also, six transmission zeros (TZs) are achieved in the operation frequency range (6–16 GHz), which improves the selectivity of the filter. The proposed filter is modeled with an approximate equivalent circuit, and the prototype of the filter is fabricated and tested to demonstrate its excellent performance. A good agreement was realized among simulation, equivalent circuit LC model, and measurement S-parameters, which proves and validates the operation of the proposed triple-band BPF. The multiple advantages of the proposed filter, such as a simple structure, compactness ($1.29\lambda_g \times 1.62\lambda_g$), selectivity, and high performance, make it a promising candidate for multi-tasking communication systems.

1. INTRODUCTION

The multiplicity of applications of wireless communication systems requires various technologies, like conventional rectangular waveguide and microstrip line for designing microwave and millimeter components such as couplers [1, 2], antennas [3, 4], and filters [5, 6], due to its characteristic properties, like low cost, small size, for microstrip line, and high Q-factor with fewer losses [7]. In contrast, these technologies have integration flaws, which become very difficult with planar structures in electronic systems and more expensive in their fabrication [8]. In the early 90's, a new technique was proposed which, instead of waveguide walls in the substrate, was based on metallic vias [9]. This technology was named substrate integrated waveguide (SIW), which takes the same previous advantages; in addition to that, it can be easily integrated with other planar circuits [10] with high power handling capacity. A SIW structure is formed by two opposite side rows of metalized vias going through a dielectric substrate, confined between two conductor planes. This structure can be used for many design components of the microwave and millimeter systems, such as filters. A filter is an important element in many radio frequency (RF), microwave, and millimeter wave systems, which removes some unwanted frequency bands or combines different frequencies [11]. It can be designed by lumped elements, like a capacitor and an inductor or by distributed elements, as planar and nonplanar waveguides, such as microstrip line, rectangular waveguide, and SIW.

With the huge emergence of new communication systems, the RF band became more overcrowded. This leads to the loss of the desired signal due to the interference with other communication system signals. To solve this problem, a filter with multiple passbands and rejected upper and lower bands is the key. Many techniques have been proposed for designing this kind of component. The most popular techniques are the combination of different frequencies of single-bandpass filters in one response [12]. The merging of complementary split-

* Corresponding author: Mohammed Boulesbaa (boulesbaa.mohammed@univ-ouargla.dz).

ring resonators (CSRRs) on the SIW cavity ceiling appeared as miniaturized multi-passband filters [13, 14]. However, the realized passbands are implemented in lower microwave band frequencies (typically lower than 10 GHz) due to the radiation characteristics of the distorted structure CSRR. Recently, triple-band bandpass filters operated in the higher frequency realized with rectangular cavities and perturbed SIW modes have been reported [15–19]. The three passbands of this filter are achieved based on the coupling between the resonant frequencies of the combined SIW cavities [15]. However, the non-flexible tuning of the center frequencies of passbands and a shortage of transmission zeros (TZs) in the stopbands can be observed due to the use of only two modes. The coupling of the TE_{101} and TE_{201} modes of the SIW cavity with a split-type dual-band symmetrical frequency response results in triple passbands at CFs, 11.578 GHz, 12.468 GHz, and 14.985 GHz, respectively, and five TZs in the rejection bands [16]. Despite the efficient performance, this technique is facing the difficulty of controlling and coupling mode excitation, which requires the careful design of perturbation structures. Two triple-band BPFs are designed in [17] with the third and fourth orders based on triple resonant modes in each filter response. The mutual coupling of the modes is achieved due to the perturbation vias situated in the center of the SIW cavities. Nevertheless, the precise control coupling of each mode is still difficult with the complexity of the structure, which affects the insertion loss of the three bands, in addition to the large size of the component. A triple band filter designed in a single SIW cavity with a whole size of $1.44\lambda_g \times 1.44\lambda_g$ was reported in [18]. The three bands are adjustable by six modes that are perturbed with vias centered in the square cavity. However, the non-independent control of the passbands was realized due to the restriction of the structure. In addition, the attenuation in the vicinity of the passbands instead of TZs may be owing to the position of the feed line ports in the single cavity. Another triple-band filter was presented in [19] based on the perturbation of four modes, TE_{101}, TE_{102}, TE_{201}, and TE_{202}, in a single cavity with two pairs of CSRRs etched on the top layer. The first passband is structured by the perturbation of the TE_{101} and TE_{201} modes. The second passband of the same filter is realized with the resonant frequency of the CSRR operated between the frequencies of the TE_{102} and TE_{201} modes, while the third one is formed depending on the commutation of the TE_{102} mode toward the TE_{202} mode. This interlocking of the modes makes the control of bandwidth and CFs more complex and creates unwanted couplings at the CSRR level units, which increases the insertion losses. Moreover, most of the above filters lack simplicity in their design or the partnership of the cavity mode coupling between their passbands. For that reason, we built the idea of a designed triple-band BPF based on independent passbands in terms of the excitation modes.

In this paper, a triple-band BPF with a simple design and compact size is reported. The proposed filter structure is based on two secondary SIW cavities stacked vertically with a main SIW cavity. The main one provides three modes: TE_{101}, TE_{201}, and TE_{301}, in addition to the suppressed mode and two TZs. This was done by placing its seven perturbation vias in the center of the main SIW cavity.

On the other hand, the secondary cavity delivers two transmission poles (TP_1 and TP_2) and TZs. Notably, the coupling of the transmission poles with the SIW cavity modes to constitute the passband is used for the first time in this paper. Each passband of the proposed filter is constituted of separate modes, which allows more flexibility in CFs tuning with adjustable bandwidth passbands. A three bandwidth passband filter is achieved with center frequencies of 6.9 GHz, 10.1 GHz, and 13.3 GHz, respectively. The 1st passband is formed by the coupling of the suppressed mode (TE_{120}) and TP_1. The 2nd passband is realized with the coupling of the TE_{101} and TE_{201} modes, while the 3rd one was achieved with the coupling of the TE_{301} mode with TP_2. Vertical CPW slots are etched onto the main SIW cavity for coupling the TE_{101} and TE_{201} modes, which realize the 2nd passband, wherein the horizontal CPW slots are embedded in the two secondary SIW cavities for controlling the 3rd passband of the proposed filter. Six TZs are realized in the out-band of the proposed triple-band BPF for increasing the selectivity of the filter response.

This article is organized as follows. Section 2 provides detailed descriptions of the proposed main SIW cavity and its modes, as well as a brief overview and analysis of the proposed secondary SIW cavity. Furthermore, the final design of the proposed SIW triple-band bandpass filter is presented. In Section 3, the modeling (LC model) of the proposed filter using an approximate equivalent circuit is established. In Section 4, the results of manufacturing the proposed filter prototype are analyzed and discussed. A comparison among the design performance, measurements, and LC model of the proposed filter is also reported. The last section provides the conclusion of this investigation concerning the proposed filter and the assessment of its performance within the context of the field.

2. PROPOSED DESIGN OF A SIW TRIPLE-BAND BANDPASS FILTER

2.1. Design of the Proposed Main SIW Cavity

The backbone of the design structure of the triple-band BPF proposed in this work is based on the main SIW cavity. The latter consists of a rectangular SIW cavity containing seven perturbation metallic vias. The seven metallic vias are distributed in the center of the structure and have the same diameter as the side wall metallic vias, as shown in Figure 1. The main SIW cavity dimensions are mentioned in Table 1. In addition, the microstrip transition lines designed on the same substrate on

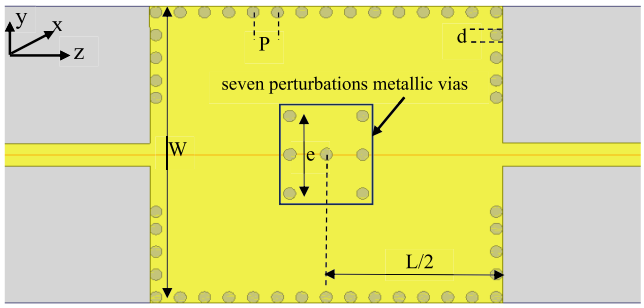

FIGURE 1. Structure of the proposed main SIW cavity.

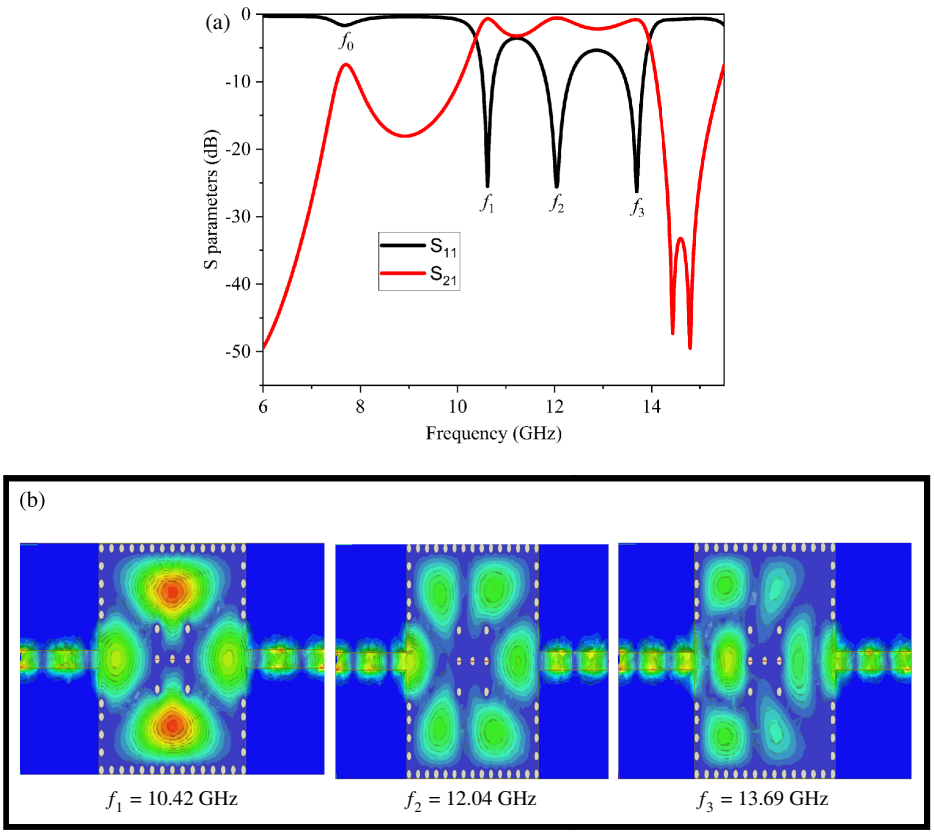

FIGURE 2. Main SIW cavity structure simulation results. (a) S-parameter results. (b) Electric current distribution at the three-mode SIW main cavity.

TABLE 1. Dimensions of the proposed main SIW cavity.

Parameter	W	L	P	e	d
Dimension (mm)	25	29	2	5.2	1

both sides are added to the SIW cavity structure. This structural composition enables electromagnetic waves to propagate within the substrate with low losses radiation, provided that the following ratio is satisfied:

$$\left(\frac{d}{P}\right) < 2.5 \tag{1}$$

where d and P are the diameter and the distance between two adjacent metallic vias, respectively.

The simulation results of the proposed design of the main SIW cavity are illustrated in Figure 2. As shown in Figure 2(a), three peaks of the S_{11} are shown in the center frequencies (CFs) $f_1 = 10.42$ GHz, $f_2 = 12.04$ GHz, and $f_3 = 13.69$ GHz. The return loss (RL) is better than 25 dB, and the insertion loss (IL) is higher than 0.3 dB. The distributions of the current at the mentioned three frequencies of the S_{11} peaks are shown in Figure 2(b). It is clear that $f_1 = 10.42$ GHz, $f_2 = 12.04$ GHz, and $f_3 = 13.69$ GHz are the CFs of the TE_{101}, TE_{201}, and TE_{301} modes, respectively. The resonant frequency of the mode cavity can be written as all well-known [19]:

$$f_{TE_{m0n}} = \frac{c}{2\pi\sqrt{\mu_r\varepsilon_r}}\sqrt{\left(\frac{m\pi}{W}\right)^2 + \left(\frac{n\pi}{L}\right)^2} \tag{2}$$

where c, μ_r, and ε_r are the light velocity in a vacuum, relative permeability, and relative permittivity, respectively, while m and n are the indices of mode at two separate axes directions in the cavity. Two transmission zeros (TZs) are generated at the frequencies 14.6 GHz and 14.8 GHz, respectively, where the first one emerged due to the bypass coupling resulting from the obstacle metallic vias, and the second one is created owing to the energy path between the input and output ports.

A suppression of the S_{21} was observed near the frequency $f_0 = 7.6$ GHz due to the overall size of the seven metallic vias in the main SIW cavity, which obstructs the distribution of the energy towards the output port. The overall size restricted a mode cavity for distributing at the frequency f_0, which represents the CF of the suppressed mode in the proposed main SIW cavity. So, the achievement of the transmission energy between the two feed line ports of the proposed main SIW cavity and realizing a response at a frequency f_0 requires a decrease of the length **e**. Figure 3 illustrates the influence of the dimension **e** on the realization of the suppression mode. A strong suppression of the reflection coefficient, S_{11}, of less than 9 dB was observed in Figure 3(a) when the dimension **e** is higher than 4.3 mm. The low return loss S_{11} equal to 23 dB is found when the dimension of the **e** is 3.2 mm. To show the mode suppressed in the proposed main SIW cavity by varying the dimension of the **e** parameter, the results of both transmission and reflection S-parameters are illustrated in Figure 3(b). As can be seen, the desired mode is decayed, and no transmission of the energy is realized at high values of the dimension **e**. Also, the CF

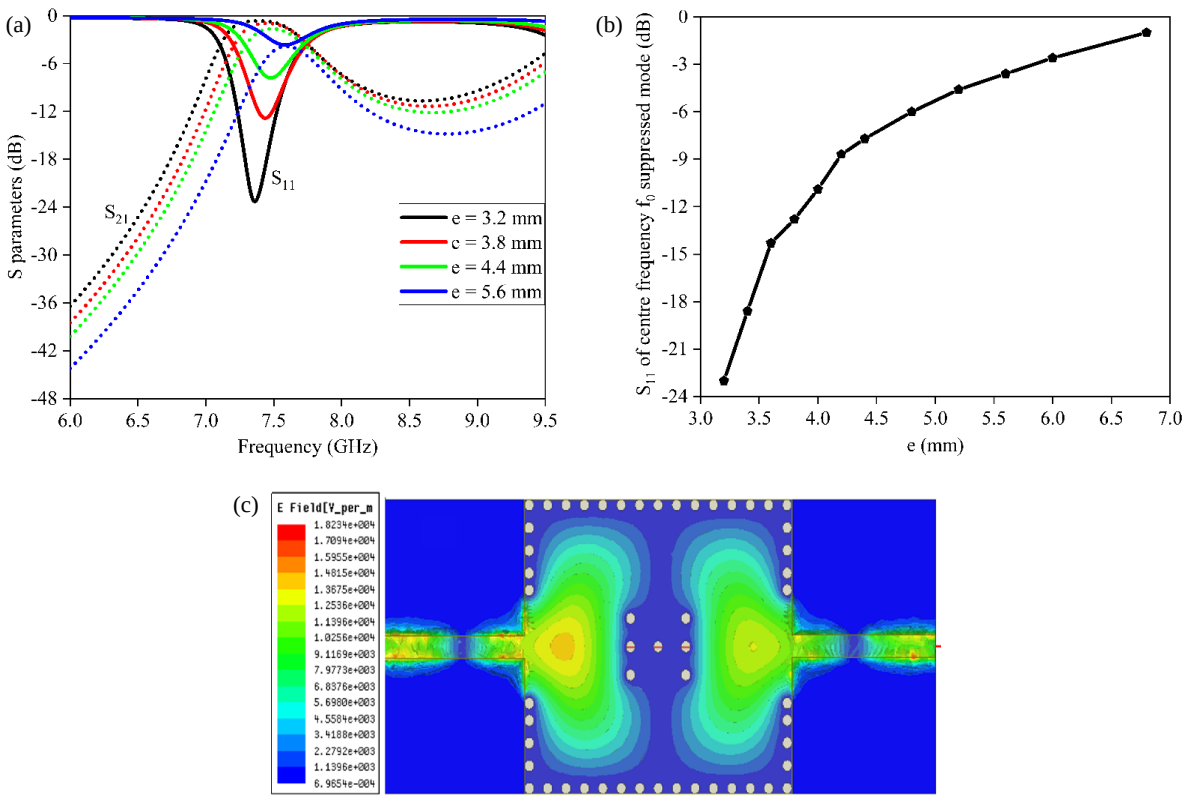

FIGURE 3. Effect of the dimension **e** on the frequency f_0 suppressed mode, (a) S_{11} and S_{21} coefficients. (b) Reflection coefficient level of the suppressed mode. (c) Current distribution extracted at a frequency f_0 (7.4 GHz).

of the suppressed mode (f_0) is tuned towards a frequency of 7.6 GHz. While the opposite happens with a decreasing value of the length **e**, the reflection coefficient reaches 23 dB at the frequency f_0 equal to 7.4 GHz with a good insertion loss of approximately 0.4 dB. A current distribution is extracted at the peak of the S_{11} (the value of the **e** is equal to 3.2 mm, and the f_0 is 7.4 GHz) and plotted in Figure 3(c). The distribution of that current between the feed lines ports at f_0 is caused by the small overall size of the proposed seven metallic vias at the center of the main SIW cavity, which marks the TE_{120} mode as identified in [20], and f_0 is determined as the center frequency of that SIW mode in this work. The main purpose of displaying the TE_{120} mode study is to know the value of the **e** parameter for which this mode was faded away or vice versa, before adding the secondary proposed SIW cavity. This is to know the behavior of the secondary SIW cavity that must be coupled with the main one, to form the SIW triple-band BPF proposed in this paper.

2.2. Proposed Design of Secondary SIW Cavity

The main idea of adding the secondary SIW cavity is to realize a coupling between its transmission poles and the modes provided by the proposed main SIW cavity. Consequently, to achieve a response of a triple-band bandpass filter, each of its bands contains two peaks of transmission, and the proposed secondary SIW cavity should have at least two transmission poles in its response. The structure design of the secondary SIW cavity is observed in Figure 4(a). It includes horizontal CPW slots on the side and six metallic via perturbations in the middle cavity, which together affect the passband characteristics of the filter. The two perturbation vias located on the side and near the CPW slots are used to affect the bandwidth of this filter. The width of the secondary SIW cavity mentioned in Figure 4(a) is equal to half of the width from the main SIW cavity ($W/2$). When two wave ports are placed at the edge of this secondary SIW cavity, the structure functions as a filter, which have a response behavior defined in terms of incident and reflected waves at ports. It is designed with the same substrate used in the design structure of the main SIW cavity, with ε_r equal to 2.94 and a thickness of 0.76 mm.

To demonstrate the coupling performance between the secondary SIW cavity and CPW slots, we study the evolution of the unloaded quality factor (Q_u) and resonance frequency (f_r) of the secondary SIW cavity with and without CPW slots. The results are illustrated in Figure 4(b). As is well known, the unloaded quality factor (Q_u) describes the energy storage capacity of a cavity relative to the rate at which it loses energy. The Q_u is expressed by the following formula [7]:

$$Q_u = 2\pi f_r \frac{E}{E_{loss}} \tag{3}$$

where E is the total energy stored in the resonance cavity, E_{loss} the total loss energy consumed by the resonance cavity, and f_r the resonance frequency of SIW cavity.

The evolution of the unloaded quality factor (Q_u) and resonance frequency (f_r) with respect to the CPW length **m** is illustrated in Figure 4(b).

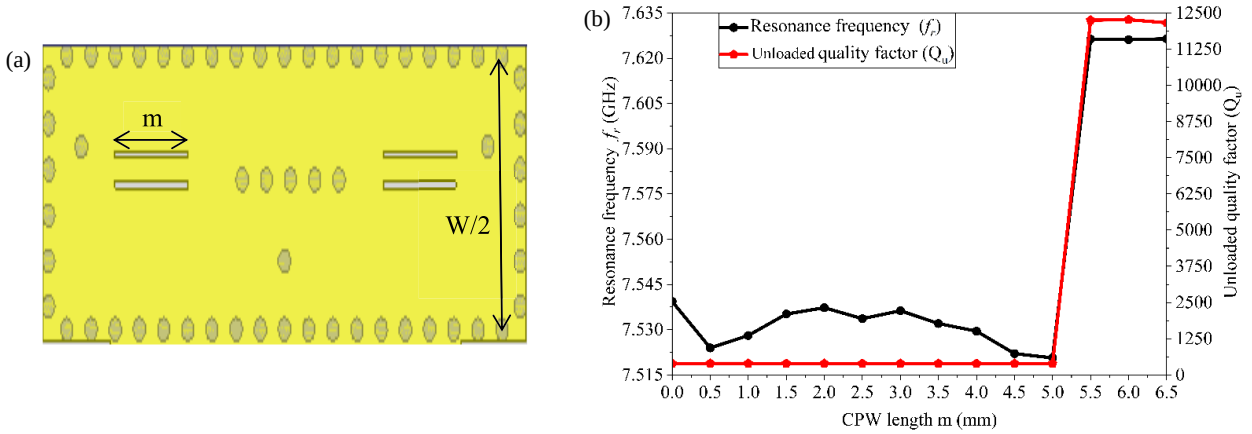

FIGURE 4. Structure of secondary SIW cavity with CPW slots, (a) design of secondary SIW cavity, (b) evolution of resonance frequency f_r and unload quality factor Q_u as a function of CPW length **m**.

As shown in Figure 4(b), the Q_u factor is very low, indicating significant energy leakage between the CPW slots and the secondary SIW cavity, while the resonance frequency changes slightly when **m** is less than 5 mm. Both curves show a transitional jump around **m** equal to 5 mm, indicating that energy leakage is minimized and efficiently stored in the cavity and that new transmission poles are created. The stability of the resonance frequency and the slight decrease in the unloaded quality factor indicate the optimal value of m at which the external load on the cavity is very small, which appears at **m** around 6 mm.

In order to demonstrate the important role that CPW slots can play in the performance of the secondary SIW cavity, we simulated the S-parameters of this cavity with and without CPW slots. The secondary SIW cavity without CPW slots was modeled with the lumped element LC circuit, as illustrated in Figure 5(a), and its comparison results of the $|S_{11}|$ and $|S_{21}|$ are plotted in Figure 5(b). As can be seen, the $|S_{11}|$ and $|S_{21}|$ results of the equivalent LC model and simulation secondary cavity without CPW slots have an identical center frequency passband of 7.75 GHz and insertion loss (IL) = 20 dB. The bandwidth frequency of the LC model filter is 0.5 GHz, higher than the simulation filter, which is 0.3 GHz.

The two TZs are observed in the simulation results created by the perturbation vias placed at the center of the main SIW cavity. Therefore, the equivalent circuit that provides transmission zero can be achieved from the parallel connection of the capacitor (C) and inductor (L) [21] with a transmission zero frequency (f_z), as expressed in the following formula [21]:

$$f_z = \frac{1}{2\pi\sqrt{LC}} \tag{4}$$

The rejection band of both compared filters observed in Figure 5(b) has two TZs at the same position frequencies, 8.9 GHz and 9 GHz, respectively, in which the $|S_{21}|$ of the LC model is recorded at zero frequencies higher than that of the simulation one, due to the radiation loss of the distribution element. So, from this comparison, it can be found that the simulated and equivalent circuit results of the S-parameters are almost perfectly consistent.

To achieve a response of the secondary SIW cavity that contains two transmission poles (TZs), the CPW slots are etched in the edge of the cavity, as shown in Figure 4(a). Therefore, these CPW slots are modeled as (capacitive) effects (C_p), approximately calculated with the modified equation proposed in [22], which is:

$$C_p \approx \frac{1}{2\pi Z_0 f_{pn}} \tag{5}$$

where Z_0 is the load impedance (50 Ω), and f_{pn} is the center frequency of the TP_n.

The addition of the CPW slots, shown in Figure 4(a), allows providing a second transmission pole (TP_2) to the response, as observed in Figure 5(c). Thus, the center frequency f_{p1} of the TP_1 is 7.75 GHz, and the center frequency f_{p2} of the TP_2 is equal to 7.82 according to the simulation results.

The approximate value of the C_p capacitor is calculated by employing Equation (5), while two of the C_p capacitors are added on the edges of the LC model illustrated in Figure 5(a), to achieve the equivalent circuit of the secondary SIW cavity with two transmission poles. The bandwidth passband has a frequency of 0.33 GHz, which can be adjusted by changing the position of the metallic vias close to the CPW slots. The two TPs (TP_1 and TP_2) of both distributed elements (design structure with substrate) and lumped elements (LC model) are approximately identical, as well as the CFs of the two TZs in the rejection band.

2.3. Final Design of the Proposed SIW Triple-Band Bandpass Filter

The operating response of the SIW triple-band BPF proposed in this paper is dependent on the coupling of the CF modes provided by the main SIW cavity with the two transmission poles of the secondary SIW cavity. The 1st bandwidth of the proposed triple-band BPF is based on the coupling of TP_1 of the secondary SIW cavity with the TE_{120} mode. While the coupling between the first and second modes of the main SIW cavity makes it possible to obtain the second bandwidth of the proposed triple-band BPF. The third bandwidth of the proposed filter can be achieved by coupling the TE_{301} mode with the TP_2.

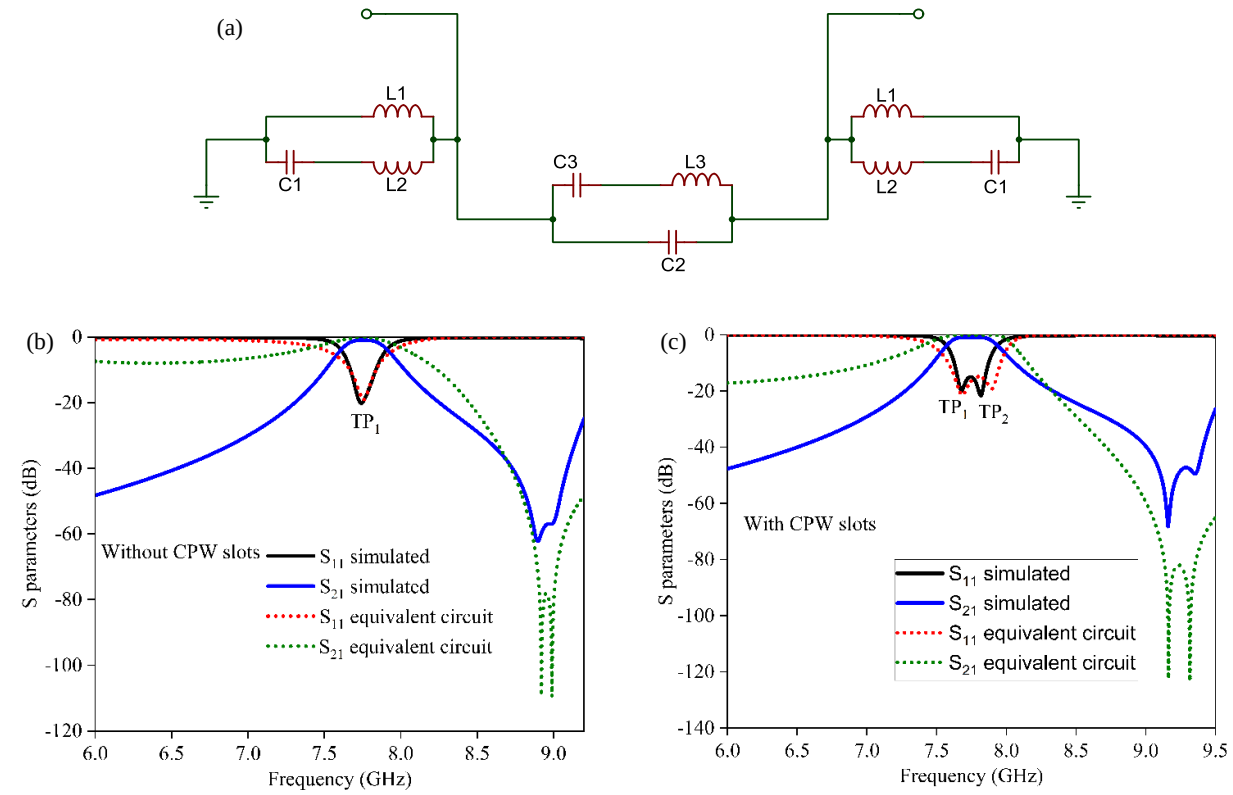

FIGURE 5. Comparison performance of the proposed secondary SIW cavity, (a) LC model of secondary SIW cavity without CPW slots (single TP), (b) comparison of $|S_{11}|$ and $|S_{21}|$ results of secondary SIW cavity without CPW slots (single TP), (c) comparison of $|S_{11}|$ and $|S_{21}|$ results of secondary SIW cavity with CPW slots (two TPs).

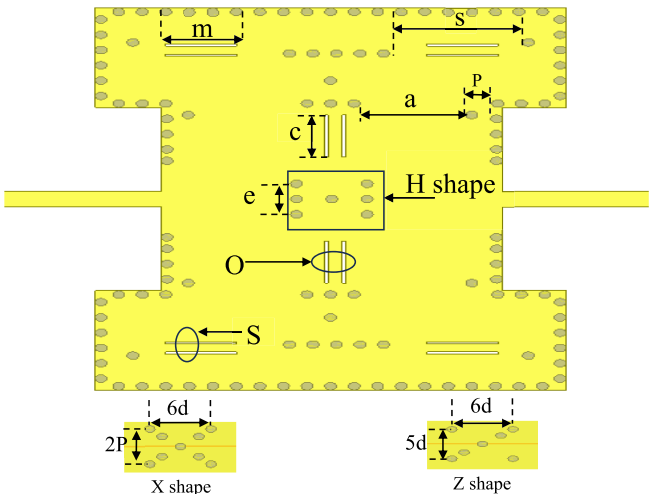

FIGURE 6. The final design of the proposed SIW triple-band bandpass filter with different H, X, and Z shapes.

The final design of the proposed SIW triple-band BPF is shown in Figure 6. It was structured on the basis of a main SIW cavity placed in the center, stacked with two other secondary SIW cavities. The connectivity of these secondary cavities is achieved through a gap indicated by the symbol "**a**", as illustrated in Figure 6.

The performance of the proposed triple-band BPF with tuning each bandwidth is shown in Figure 7. The 1st passband has a narrow bandwidth compared to the other ones of the proposed SIW triple-band BPF. It contains only one transmission peak in its response, and its center frequency is 7.05 GHz. The current distribution of the 1st passband is depicted in Figure 8(a). As we can see, the current distribution extracted in the 7.05 GHz frequency looks almost like TE_{120} mode (see Figure 3(c)), which is why it is generated close to its center frequency f_0. Although the value of the **e** dimension equals to 5.2 mm "TE_{120} mode suppressed" as we saw before in the main SIW cavity study. The use of the vertical CPW slots and gap **a** distorted the distribution of the current of the TE_{120} mode, as seen in Figure 8(a).

This distortion yields a nonuniform flow of energy in the SIW modes, which means that the current extracted at 7.05 GHz is the CF of TP_1 (f_{p1}), provided by the secondary SIW cavities. So, the tuning of the 1st passband depends on the control of the amount of energy via the gap **a**. On the other hand, by adjusting this parameter, it is possible to control the frequency of the other two bandwidths (the second and third bandwidths) of the triple-band BPF proposed. So, to achieve an independent tuning of the 1st passband, three shapes (H, X, and Z) of the position perturbation metallic vias are used, as illustrated in Figure 6. The triple SIW BPF structure with H shape exhibited the best return loss near 24 dB and insertion loss equal to 0.8 dB, as can be seen in Figure 7(a). The response of the 1st passband of the proposed triple BPF filter and the current distribution at their center frequency (TP_1) are presented in Figures 7(a) and 8(a).

The 2nd bandwidth of the proposed filter is formed by coupling the CFs of TE_{101} and TE_{201} as exhibited in Figure 7(b), and the current extracted is shown in Figures 8(b) and (c). The

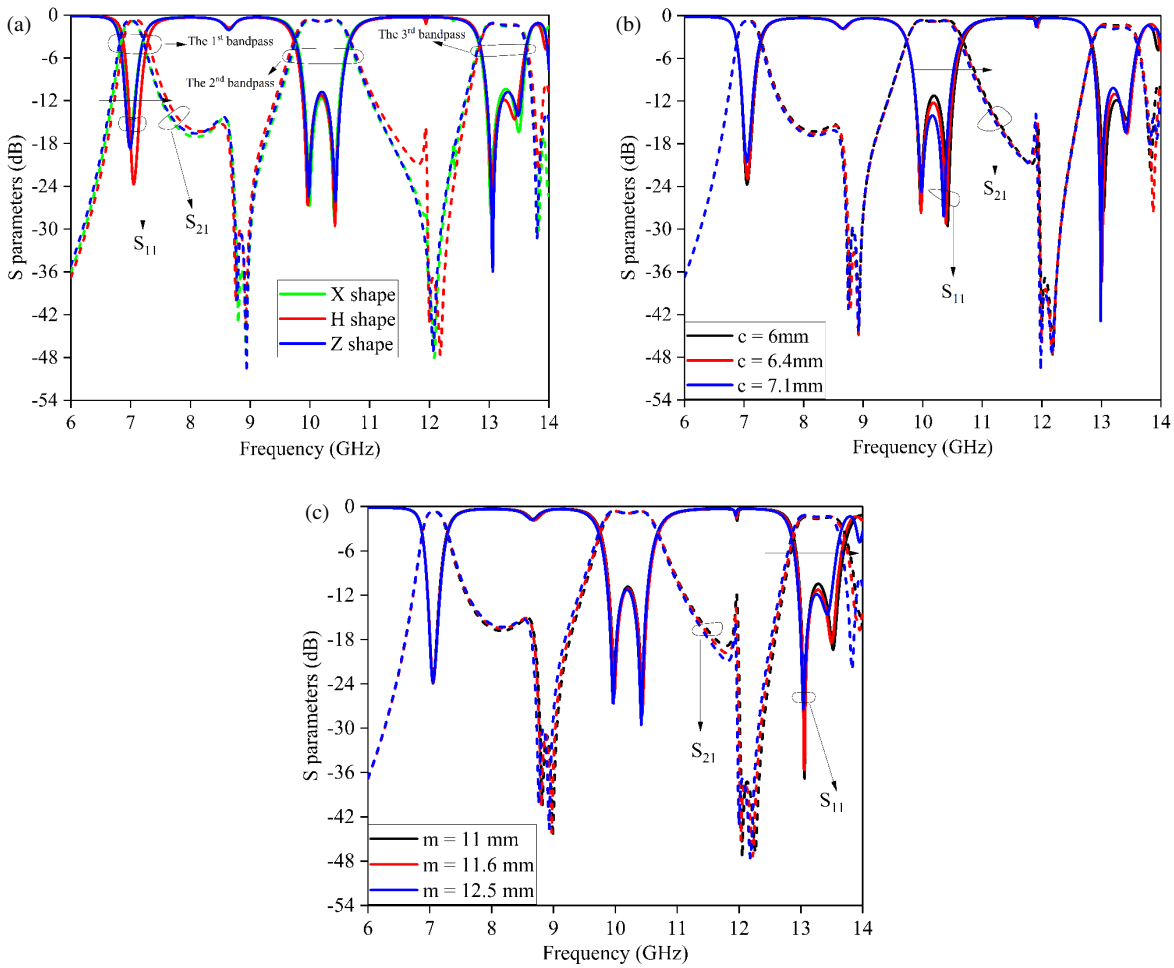

FIGURE 7. The $|S_{11}|$ and $|S_{21}|$ of proposed triple-band BPF, (a) tuning of the first passband, (b) tuning of the second passband, (c) tuning of the third passband.

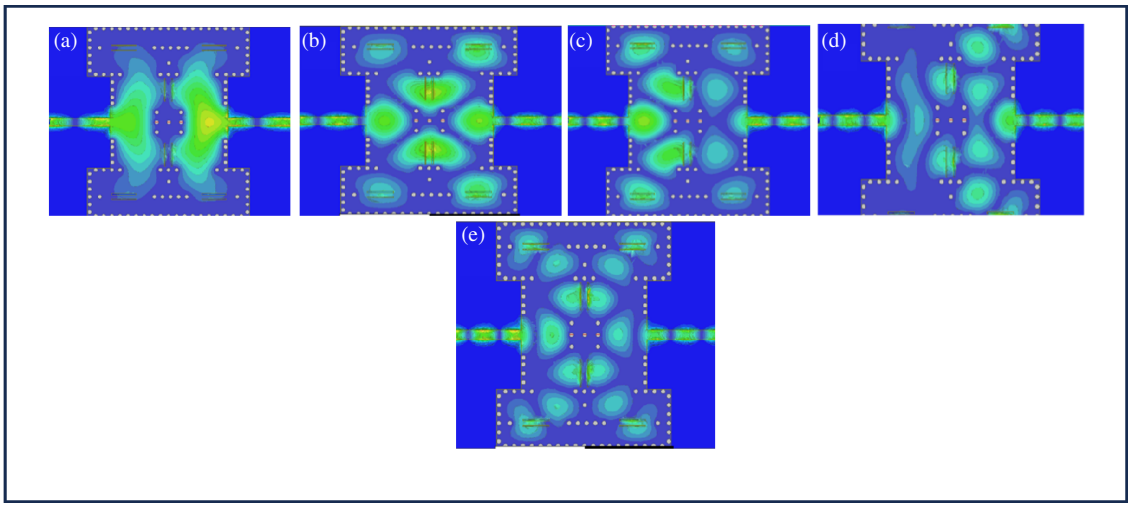

FIGURE 8. Current distribution of the proposed SIW triple-band BPF, (a) electric field TP_1 at 7.05 GHz, (b) electric field mode 1 at $f_1 = 9.97$ GHz, (c) electric field mode 2 at $f_2 = 10.42$ GHz, (d) electric field TP_2 at 13.04 GHz, (e) electric field mode 3 at $f_3 = 13.43$ GHz.

tuning of the second passband is based on the shifting of the f_2 with the length of the vertical CPW slots (section O, Figure 6). As we can see from Figure 7(b), the increase of the **c** value leads to moving the f_2 frequency towards the f_1 of mode 1, which means that a strong coupling between the two modes of the main SIW cavity is achieved. A small effect occurs on the first peak of the 3rd bandwidth due to the closeness of the length CPW slots **c** on gap **a**. This peak represents the center frequency

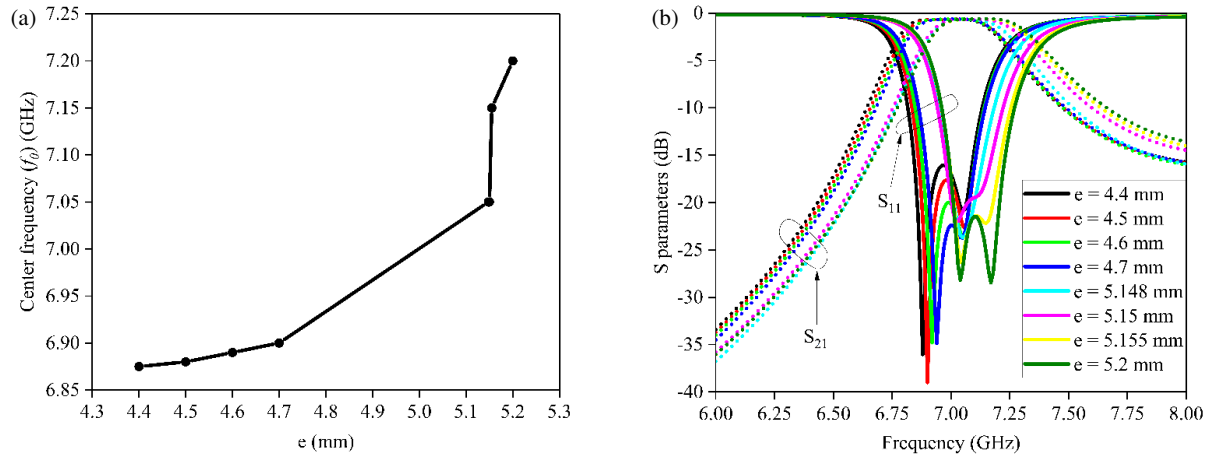

FIGURE 9. Effect of dimension **e** on the 1st passband bandwidth of the proposed triple-band BPF, (a) variation of center frequency (f_0) of TE_{120} mode as a function of **e**, (b) $|S_{11}|$ and $|S_{21}|$ of 1st passband bandwidth at different values of **e**.

(f_{p2}) of TP_2, which is demonstrated by the inconsistency of the current depicted in Figure 8(d). A tuning of the third passband is shown in Figure 7(c). The 3rd passband of the proposed triple-band BPF was created depending on the coupling of the third mode f_3 (see Figure 8(e)) with the transmission pole TP_2 (see Figure 8(d)), where the stack of the two secondary cavities with the main SIW cavity of the proposed filter shifted TP_2 near the frequency of 13.1 GHz, and a new frequency f_3 was created near 13.6 GHz, as displayed in Figure 7.

The extension of the bandwidth of the 3rd passband filter is done by coupling the CF of the transmission pole TP_2 (f_{p2}) with the f_3 frequency (13.43 GHz), which is created by the optimization of the horizontal CPW slots length **m** (section S, Figure 6). The control of the 3rd passband filter is done by moving the frequency f_3, as can be seen in Figure 7(c).

For enhancing the performance of the proposed triple-band BPF, we optimized the three bandwidths of this component, depending on the metallic vias perturbation and the CPW slots used in the filter's structure. The optimization of each passband bandwidth of the triple-band BPF is presented in the next section of this work.

2.3.1. Adjustment of the 1st Passband of the Triple-Band BPF

From the extracted S-parameter results of the proposed filter presented in Figure 7, it can be seen that the 1st passband has a narrow bandwidth (one transmission pole TP_1). However, the proposed triple-band BPF, which includes an H-shaped pattern, has exhibited good performance in terms of the passband compared to the other shape patterns. To extend the 1st bandwidth passband of the proposed filter, a coupling between the CFs of the TE_{120} mode and TP_1 should be achieved. For this, the parameter **e** appearing in Figure 6 can be optimized, as previously discussed in the first section. The obtained results are presented in Figure 9.

Figure 9(a) presents the influence of the dimension **e** on the center frequency f_0 of the TE_{120} mode at the response of the 1st passband bandwidth triple-band BPF. The choice of the values of parameter **e** depends on the previous study of the TE_{120} mode in the first part. As we can observe from Figure 9(b), the center frequency of TP_1 is approximately the same as that of the f_0 at two values of the length **e**, which are 5.148 mm and 5.15 mm, respectively. This indicates that there is a strong coupling between TP_1 of secondary SIW cavities and TE_{120} mode of the main SIW cavity. The strong coupling of TE_{120} with TP_1 enabled a narrow passband with a 0.3 GHz bandwidth. The high control of f_0 by changing the length **e** achieves an adjustable bandwidth of the 1st passband of the proposed filter. The values of $\mathbf{e} < 5.148$ mm shifted the f_0 towards low frequencies ($f_0 < f_{p1}$), and the values of $e > 5.15$ mm shifted the f_0 towards high frequencies ($f_0 > f_{p1}$), as depicted in Figure 9(b). The proposed triple BPF filter takes a broad bandwidth of 1st passband with two values of the dimension **e**, 4.4 mm and 5.2 mm. The bandwidths of the 1st passband are 0.5 GHz and 0.48 GHz at the previous dimensions of the **e**, respectively. Also, the RL is higher than 15 dB, and IL is greater than 0.3 dB.

2.3.2. Adjustment of the 2nd Passband of the Triple-Band BPF

The 2nd passband bandwidth filter depends on the coupling between the CFs f_1 and f_2 of the main SIW cavity, whilst the coupling of frequencies f_1 and f_2 is done by adding two secondary SIW cavities with a gap of **a**. The highlight of a passband formed by modes is the flexibility in controlling the bandwidth, which is due to the independent tuning of one of these modes. The control of the second mode was done with the length of the vertical CPW slots **c** depicted in Figure 6 (section O). The influence of length **c** on the frequency f_2 is illustrated in Figure 10(a). As we can see, the variation in dimension **c** leads to a variation in the f_2 of mode 2 while the f_1 of mode 1 remains approximately unchanged. In contrast, the increase in length **c** is accompanied by a high coupling between the frequencies f_1 and f_2 of the modes, and the bandwidth is 0.9 GHz, as seen in the S-parameter results in Figure 10(b). The IL of the 2nd passband is better than 0.3 dB, and RL is higher than 15 dB with a value of **c** equal to 6.9 mm. Tuning f_2 to the frequency 10.5 GHz extends the bandwidth of the 2nd passband, which increases by 0.2 GHz. Also, good return loss (higher than 10 dB)

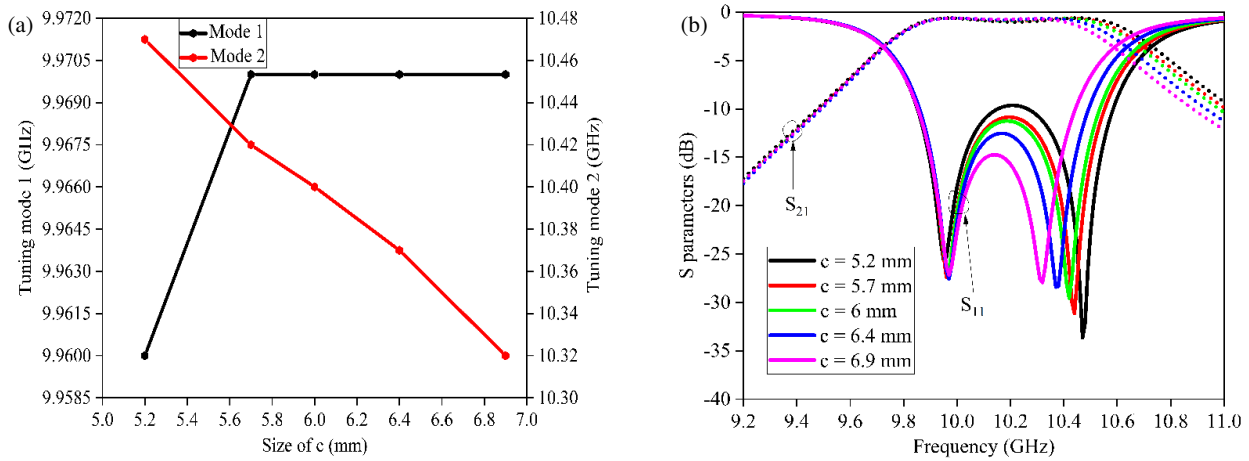

FIGURE 10. Effect of dimension **c** on the 2nd passband of the proposed triple-band BPF, (a) variation of center frequencies modes f_1 and f_2 as a function of **c**, (b) adjustable bandwidth S-parameters of the 2nd passband at various dimensions of **c**.

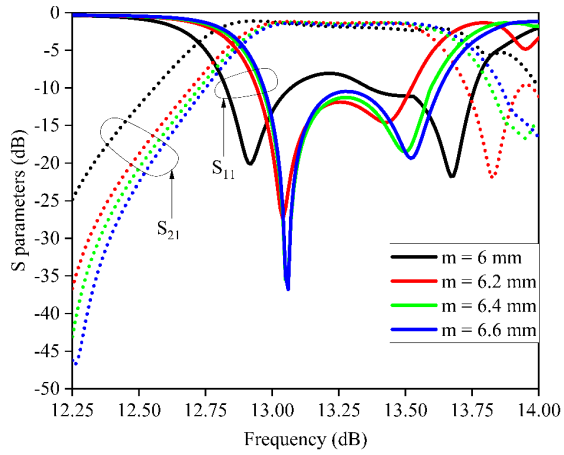

FIGURE 11. Effect of dimension **m** on the S-parameters 3rd passband of the proposed triple-band BPF.

and insertion loss (0.3 dB) are obtained with **c** equal to 5.2 mm and f_2 at 10.5 GHz.

2.3.3. Adjustment of the 3rd Passband of the Triple-Band BPF

The addition of the two secondary SIW cavities to the main SIW cavity for structuring the SIW triple-band BPF leads to the formation of 3rd passband with two S_{11} peaks in the bandwidth, whose positions are indicated at frequencies f_{p2} and f_3. The control of the bandwidth of the 3rd passband can be applied by adjusting f_3, which is achieved by varying the length of the horizontal CPW slots (named **m**) shown in Figure 6. The effect of this parameter on the third passband of the triple-band BPF is observed in Figure 11. The extension of the bandwidth is more closely related to the inverse shifting of f_3 with respect to the frequency f_{p2}, which is realized when **m** is 6.2, 6.4, and 6.6 mm. A bandwidth of 1.2 GHz of the 3rd passband and a center frequency equal to 13.3 GHz were observed by shifting both f_3 and TP_2. This is caused by the change in dimension **s** between the perturbation metallic vias of the secondary cavity, which is equal to 12.3 mm and the length **m** (**m** = 6 mm).

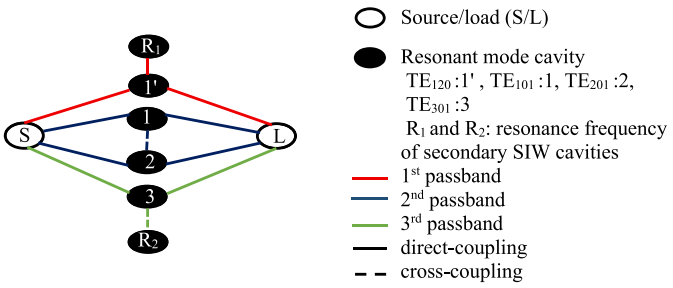

FIGURE 12. Equivalent coupling topology of the proposed SIW triple-band BPF.

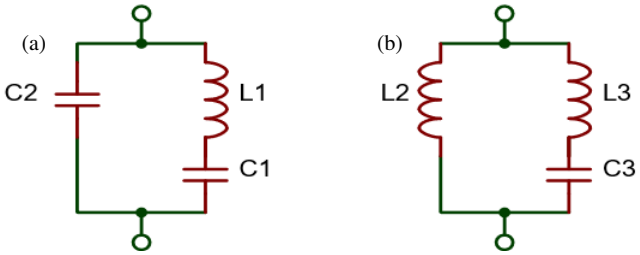

FIGURE 13. LC model resonator, (a) first branch ($L1$ and $C1$ connected in series) and parallel connected with $C2$, (b) second branch ($L3$ and $C3$ connected in series) and parallel connected with $L2$.

To illustrate the performance of operating modes and resonant frequencies cavity of the three passbands of the proposed filter, coupling topology is presented in Figure 12.

The mode resonator TE_{120} operates near the first resonance frequency of the secondary SIW cavity at the CF of the 1st passband by direct coupling through a window named **a** (as shown in Figure 6). The cross coupling implemented by the CPW slots (section O in Figure 6) allows operating the two modes of the main SIW cavity (TE_{101} and TE_{201}) at the CF of the 2nd passband of the proposed filter, where the horizontal CPW slots (section S in Figure 6) allow the TE_{301} to operate near the second resonance frequency of the secondary SIW cavity by negative direction coupling at the CF of the 3rd passband of the proposed filter.

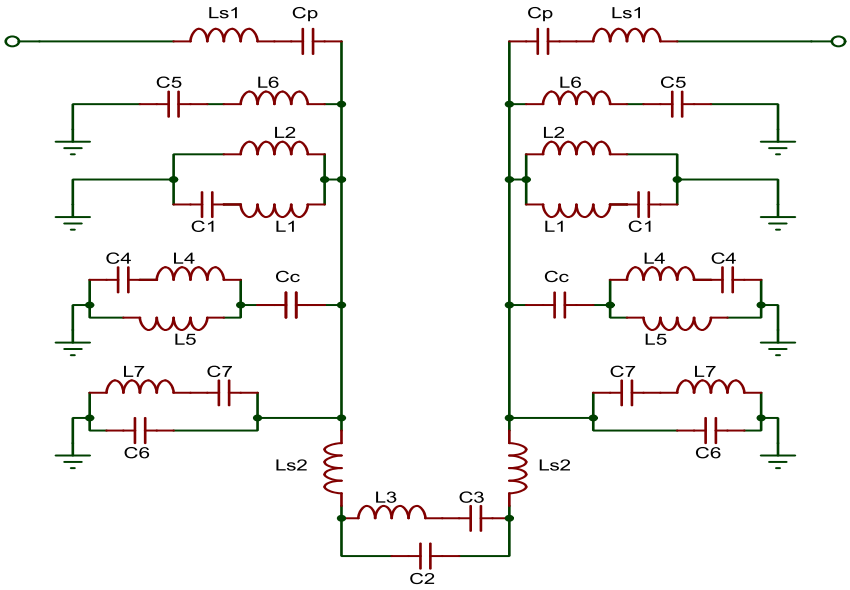

FIGURE 14. Approximate LC model circuit of the proposed SIW triple-band BPF.

3. APPROXIMATE EQUIVALENT CIRCUIT OF THE PROPOSED TRIPLE-BAND BPF

Similar to the achievement of a triple-band BPF using distributed elements, we modeled the behavior of this proposed filter by forming an equivalent circuit using lumped elements. The transmitting poles and transmitting zeros of the LC circuit filter are usually formed by a combination of an inductor (L) and a capacitor (C) connected in parallel. The determination of L and C values depends on the position of the resonance frequency f_r, which is expressed by:

$$f_r = \frac{1}{2\pi\sqrt{LC}} \tag{6}$$

As far as we know, the above LC resonator is more effective on the narrow stopband (zeros) and also narrow passband (poles). For that, we modeled each passband of the proposed filter with two branches. The first branch combines an inductor ($L1$) and a capacitor ($C1$) in series, in parallel with a capacitor ($C2$), while the second branch contains a capacitor ($C3$) in series with an inductor ($L3$). Both branches are connected in parallel with an inductor ($L2$), as shown in Figure 13.

The resonance frequency in each case is represented by the following formula:

For case (a)

$$f_{r1} = \frac{1}{2\pi\sqrt{\frac{C1\cdot C2}{C1+C2} \times L1}} \tag{7}$$

For case (b)

$$f_{r2} = \frac{1}{2\pi\sqrt{C3\,(L2+L3)}} \tag{8}$$

Thereby to form an approximate LC model circuit exhibiting the same behavior as the proposed triple-band BPF, a combination between the LC resonators, as shown in Figure 13, is structured. The coupling of these LC resonators is done by means of a coupling capacitance (Cc) and a shunt inductance (Ls) between them, while Ls and Cc take small values depending on the passband and bandwidth of the independent resonators of the filter. The schematic of the approximate equivalent LC model of the proposed triple-band BPF is illustrated in Figure 14.

4. RESULTS AND DISCUSSION

For highlighting the purpose of the above study, the triple-band BPF proposed in this work was fabricated. The type of the substrate employed to fabricate the proposed filter is RT/duroid 6002 with the following characteristics: relative dielectric constant of 2.94 and thickness of 0.76 mm. The final dimensions of the filter are **W** = 15 mm, **L** = 29 mm, **P** = 2 mm, **a** = 9 mm, **c** = 5.2 mm, **d** = 1 mm, **m** = 6 mm, **e** = 4.4 mm, and **s** = 12.3 mm.

A photograph of the fabricated triple-band BPF, with a comparison results of the simulated, equivalent circuit, and measured S parameters, is shown in Figure 15. According to Figure 15(b), the measurements carried out on the first, second, and third passbands exhibit center frequencies of 6.9/10.1/13.3 GHz with FBW 7.6%/12.2%/7.4%, respectively. The in-band return loss of each passband is better than 9 dB, while the maximum measurement insertion losses of the three bands are 0.8/0.9/2 dB, as shown in Figure 15(b). Identical measured and simulated TZ frequencies are observed in the three passbands, which indicates the high suppression of unwanted frequencies. Also, an acceptable performance of triple-band BPF LC model circuit is achieved compared with the fabricated and simulation filter. It denotes a good analysis between the performance of lumped and distributed elements. All these comparison results indicate the effective performance of the proposed filter and its ability to work in the field of multi-application telecommunication systems.

TABLE 2. Comparison between the performances of the proposed design and some triple-band BPF.

Ref.	No. Layer	Type	Center freq. [GHz]	3 dB FBW [%]	IL [dB]	No. TZ	ADI	Size (λ_g^2)	LC Model filter
[17], 2018	single	SIW	13 14 15	2.8 2.5 2.2	1.71 1.8 2.29	3	No	3.38×1.19	No
			11 12 13	2.3 1.7 2	2.02 2.72 2.57	7		2.20×2.20	
[23], 2018	three	SIW MSL	2.33 5.08 29.6	17.6 11.81 7.7	0.75 0.89 2.8	/	No	0.46×0.21	No
[24], 2019	two	SIW	6.5 7.35 8.15	2.31 2.04 2.45	1.74 1.82 1.96	6	No	1.91×0.57	No
[25], 2021	single	SIW	8.02 11.44 12.52	1.35 3.58 3.39	1.91 1.35 1.43	4	No	1.11×1.11	No
			7.7 11.0 12.1	4.63 3.40 3.14	1.98 2.01 2.15	/		1.52×1.52	
[26], 2024	single	SSPP	1.45 3.43 4.45	200 24.8 24.2	0.8	/	No	0.47×0.05	No
[27], 2025	single	SIW SSPP	24.65 26.95 29.3	5.27 7.05 4.77	0.5 0.7 0.8	/	No	1.68	No
This work	**single**	SIW	6.9 10.1 13.3	7.6 12.2 7.4	0.8 0.9 2	**6**	**Yes**	$\mathbf{1.29 \times 1.62}$	**Yes**

Footnote: MSL: Microstrip line, SSPP: Spoof Surface Plasmon Polaritons, FBW: Fractional Bandwidth, IL: Insertion loss, ADI: Adjustable bandwidth independently TZ: Transmission zero, λ_g: The guided wavelength, LC: Inductor capacitor.

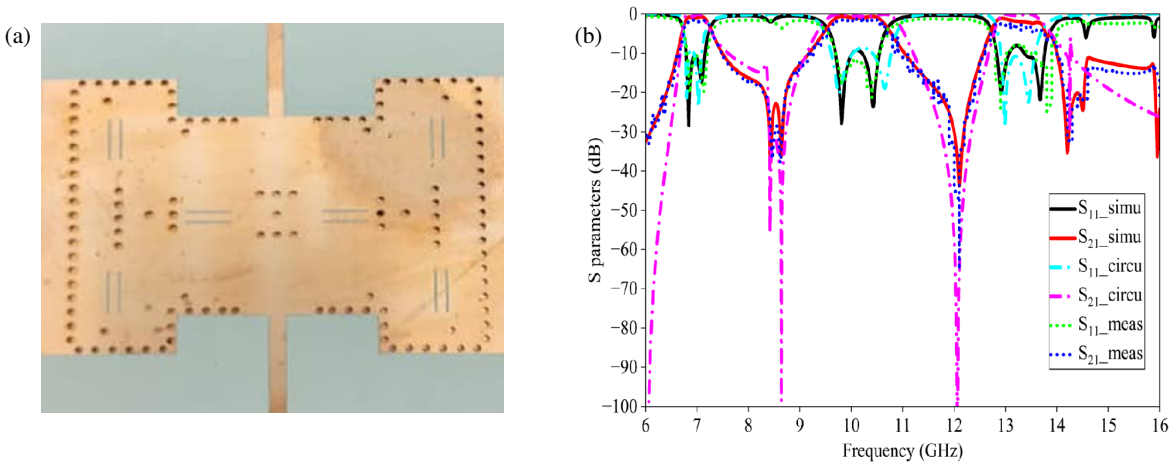

FIGURE 15. Proposed SIW triple-band BPF, (a) experimental photograph of the fabricated SIW filter, (b) comparison results of simulated, equivalent circuit and measured S-parameters.

A comparison between the performances of the proposed triple-band BPF and those of the other previous filters presented in the literature is conducted, as tabulated in Table 2. The proposed filter has a good IL and excellent rejection stopbands with six TZs. In addition, the proposed triple-band BPF represents a simple compact structure size with a flexible assignment of bands, due to the perturbation cavities.

5. CONCLUSION

In this work, a new design structure of a triple-band BPF based on one main and two secondaries planar SIW cavities was proposed. The four modes of the main cavity realized by the seven-perturbation metallic vias were considered as a backbone of the three passbands of the proposed filter. The two secondary cavities were used to achieve flexibility and independent bandwidth passbands of the proposed filter. The three-operation ranges of the proposed triple-band BPF are [6.71 GHz–7.24 GHz], [9.50 GHz–10.8 GHz], and [12.69 GHz–13.89 GHz] with good IL (above 2 dB) and RL (less than 10 dB) in each passband. The proposed SIW triple-band BPF was modeled with an LC circuit model and validated by fabrication, and its performance was measured and compared with the simulation results. A good agreement among simulation, experiment, and the LC circuit model results is obtained, due to the simple filter design and its good performance. The flexibility of passbands and the compact size of the proposed filter open up opportunities for using it in multifunctional communication applications.

ACKNOWLEDGEMENT

The authors are deeply grateful to the centre-Énergie Matériaux Télécommunication, Institut national de la recherche scientifique (INRS), Montréal (Québec), Canada, for fabricating the prototypes and carrying out the measurements.

REFERENCES

[1] Jia, H., K. Yoshitomi, and K. Yasumoto, "Rigorous and fast convergent analysis of a rectangular waveguide coupler slotted in common wall," *Progress In Electromagnetics Research*, Vol. 46, 245–264, 2004.

[2] Sun, K.-O., S.-J. Ho, C.-C. Yen, and D. Van Der Weide, "A compact branch-line coupler using discontinuous microstrip lines," *IEEE Microwave and Wireless Components Letters*, Vol. 15, No. 8, 519–520, 2005.

[3] Elsherbini, A. and K. Sarabandi, "Compact directive ultra-wideband rectangular waveguide based antenna for radar and communication applications," *IEEE Transactions on Antennas and Propagation*, Vol. 60, No. 5, 2203–2209, 2012.

[4] Aboualalaa, M., A. B. Abdel-Rahman, A. Allam, H. Elsadek, and R. K. Pokharel, "Design of a dual-band microstrip antenna with enhanced gain for energy harvesting applications," *IEEE Antennas and Wireless Propagation Letters*, Vol. 16, 1622–1626, 2017.

[5] Zhao, X. H., J. F. Bao, G. C. Shan, Y. J. Du, Y. B. Zheng, Y. Wen, and C. H. Shek, "D-band micromachined silicon rectangular waveguide filter," *IEEE Microwave and Wireless Components Letters*, Vol. 22, No. 5, 230–232, 2012.

[6] Shen, W., X.-W. Sun, and W.-Y. Yin, "A novel microstrip filter using three-mode stepped impedance resonator (TSIR)," *IEEE Microwave and Wireless Components Letters*, Vol. 19, No. 12, 774–776, 2009.

[7] Pozar, D. M., *Microwave Engineering: Theory and Techniques*, John Wiley & Sons, 2005.

[8] Rhbanou, A., M. Sabbane, and S. Bri, "Design of dual-mode substrate integrated waveguide band-pass filters," *Circuits and Systems*, Vol. 6, No. 12, 257–267, 2015.

[9] Pilote, A. J., K. A. Leahy, B. A. Flanik, and K. A. Zaki, "Waveguide filters having a layered dielectric structure," U.A. Patent, No. 5, 382931, Jan. 1995.

[10] Boulesbaa, M., T. Djerafi, A. Bouchekhlal, and B. Mekimah, "Design of a directional coupler based on SIW technology for X band applications," in *2020 1st International Conference on Communications, Control Systems and Signal Processing (CCSSP)*, 85–89, El Oued, Algeria, 2020.

[11] Hong, J.-S. G. and M. J. Lancaster, *Microstrip Filters for RF/Microwave Applications*, John Wiley & Sons, 2004.

[12] Wu, L.-S., J.-F. Mao, W.-Y. Yin, and Y.-X. Guo, "A dual-band filter using stepped-impedance resonator (SIR) embedded into substrate integrated waveguide (SIW)," in *2010 IEEE Electrical Design of Advanced Package & Systems Symposium*, 1–4, Singapore, 2010.

[13] Dong, Y., C. T. M. Wu, and T. Itoh, "Miniaturised multi-band substrate integrated waveguide filters using complementary split-ring resonators," *IET Microwaves, Antennas & Propagation*, Vol. 6, No. 6, 611–620, 2012.

[14] Zhang, H., W. Kang, and W. Wu, "Miniaturized dual-band differential filter based on CSRR-loaded dual-mode SIW cavity," *IEEE Microwave and Wireless Components Letters*, Vol. 28, No. 10, 897–899, 2018.

[15] Guo, X., L. Zhu, and W. Wu, "Design method for multiband filters with compact configuration in substrate integrated waveguide," *IEEE Transactions on Microwave Theory and Techniques*, Vol. 66, No. 6, 3011–3018, 2018.

[16] Zhou, K., C. Zhou, and W. Wu, "Substrate-integrated waveguide triple-band filter with improved frequency and bandwidth allocations," *Electronics Letters*, Vol. 54, No. 19, 1132–1134, 2018.

[17] Xie, H.-W., K. Zhou, C.-X. Zhou, and W. Wu, "Substrate-integrated waveguide triple-band bandpass filters using triple-mode cavities," *IEEE Transactions on Microwave Theory and Techniques*, Vol. 66, No. 6, 2967–2977, 2018.

[18] Liu, Y.-J., G. Zhang, S.-C. Liu, and J.-Q. Yang, "Compact triple-band filter with adjustable passbands on one substrate integrated waveguide square resonant cavity," *Microwave and Optical Technology Letters*, Vol. 62, No. 12, 3709–3715, 2020.

[19] Li, D., W. Luo, X. Chen, Y. Liu, K.-D. Xu, and Q. Chen, "Miniaturized dual-/tri-/quad-band bandpass filters using perturbed multimode SIW cavity," *IEEE Transactions on Components, Packaging and Manufacturing Technology*, Vol. 13, No. 10, 1685–1693, 2023.

[20] Namanathan, P. and G. Nagarajan, "Realization of dual-mode, high-selectivity SIW cavity bandpass filter by perturbing circular shape vias," *Applied Physics A*, Vol. 128, No. 9, 773, 2022.

[21] Lin, L.-J., M.-H. Ho, and W.-Q. Xu, "Design of compact suspended stripline bandpass filters with wide stopband," *Microwave and Optical Technology Letters*, Vol. 50, No. 4, 865–868, 2008.

[22] Omar, A. A., N. I. Dib, K. Hettak, M. C. Scardelletti, and R. M. Shubair, "Design of coplanar waveguide elliptic low pass filters," *International Journal of RF and Microwave Computer-Aided Engineering*, Vol. 19, No. 5, 540–548, 2009.

[23] Zheng, S. Y., Z. L. Su, Y. M. Pan, Z. Qamar, and D. Ho, "New dual-/tri-band bandpass filters and diplexer with large frequency ratio," *IEEE Transactions on Microwave Theory and Techniques*, Vol. 66, No. 6, 2978–2992, 2018.

[24] Yang, Z., B. You, and G. Luo, "Dual-/tri-band bandpass filter using multimode rectangular SIW cavity," *Microwave and Optical Technology Letters*, Vol. 62, No. 3, 1098–1102, 2020.

[25] Zhang, J., Q. Liu, D. Zhou, and D. Zhang, "Single- and triple-band bandpass filters using novel perturbed isosceles right-angled triangular SIW cavities," *IET Microwaves, Antennas & Propagation*, Vol. 15, No. 3, 241–252, 2021.

[26] Ren, B., C. Qin, and X. Guan, "Compact dual- and triple-wideband filters using interdigital spoof surface plasmon polaritons," *IEEE Microwave and Wireless Technology Letters*, Vol. 35, No. 1, 51–54, 2025.

[27] Liao, Q., G. Tang, T. Xiao, C. Liu, L. Huang, and H. Wang, "Design of 5G-advanced and beyond millimeter-wave filters based on hybrid SIW-SSPP and metastructures," *Electronics*, Vol. 14, No. 15, 3026, 2025.